Muscular Basis of Whisker Torsion in Mice and Rats

SEBASTIAN HAIDARLIU,* KNARIK BAGDASARIAN, NAMRATA SHINDE, AND EHUD AHISSAR

Department of Neurobiology, The Weizmann Institute of Science, Rehovot, Israel

ABSTRACT

Whisking mammals move their whiskers in the rostrocaudal and dorsoventral directions with simultaneous rolling about their long axes (torsion). Whereas muscular control of the first two types of whisker movement was already established, the anatomic muscular substrate of the whisker torsion remains unclear. Specifically, it was not clear whether torsion is induced by asymmetrical operation of known muscles or by other largely unknown muscles. Here, we report that mystacial pads of newborn and adult rats and mice contain oblique intrinsic muscles (OMs) that connect diagonally adjacent vibrissa follicles. Each of the OMs is supplied by a cluster of motor end plates. In rows A and B, OMs connect the ventral part of the rostral follicle with the dorsal part of the caudal follicle. In rows C–E, in contrast, OMs connect the dorsal part of the rostral follicle to the ventral part of the caudal follicle. This inverse architecture is consistent with previous behavioral observations [Knutsen et al.: Neuron 59 (2008) 35–42]. In newborn mice, torsion occurred in irregular single twitches. In adult anesthetized rats, microelectrode mediated electrical stimulation of an individual OM that is coupled with two adjacent whiskers was sufficient to induce a unidirectional torsion of both whiskers. Torsional movement was associated with protracting movement, indicating that in the vibrissal system, like in the ocular system, torsional movement is mechanically coupled to horizontal and vertical movements. This study shows that torsional whisker rotation is mediated by specific OMs whose morphology and attachment sites determine rotation direction and mechanical coupling, and motor innervation determines rotation dynamics. Anat Rec, 300:1643–1653, 2017. © 2017 Wiley Periodicals, Inc.

Key words: mystacial pad; oblique intrinsic muscles; electrical microstimulation; whisker; whisking; torsion; rodents

This article was published online on 27 June 2017. After online publication, minor revisions were made to the text. This notice is included in the online and print versions to indicate that both have been corrected on 10 July 2017.

Abbreviations: CCO = cytochrome oxidase; EM = extrinsic muscle; FM = follicular intrinsic muscle; MP = mystacial pad; OM = oblique intrinsic muscle; SM = straddling intrinsic muscle.

Grant sponsor: The Israel Science Foundation, Grant number: 1127/14; Grant sponsors: The Minerva Foundation funded by the Federal German Ministry for Education and Research; The Israel Ministry of Defense and the United States-Israel Binational Science Foundation (BSF), Grant number: 2011432. E.A. holds the Helen Diller Family Professorial Chair of Neurobiology.

*Correspondence to: Sebastian Haidarliu, Department of Neurobiology, The Weizmann Institute of Science, Rehovot 76100, Israel. Tel.: 972-8-9342192. Fax: 972-8-9344131 E-mail: sebastian.haidarliu@weizmann.ac.il

Received 2 October 2016; Revised 16 December 2016; Accepted 10 January 2017.

DOI 10.1002/ar.23623

Published online 16 June 2017 in Wiley Online Library (wileyonlinelibrary.com).

INTRODUCTION

Whisker movements in active rat were first described by Vincent (1912) and later characterized as recurrent whisker protraction and retraction by Welker (1964). Then Bermejo and colleagues (Bermejo et al., 2002) found that these large sweeping rostrocaudal whisker movements are coupled with smaller dorsoventral movements. Moreover, whisking appeared to be permanently coupled also with rolling of the whiskers about their own axes (whisker torsion, Knutsen et al., 2008). Rostral whisker movement, or protraction, is initiated by contraction of the medial inferior and medial superior parts of the extrinsic muscle (EM) *M. nasolabialis profundus* and completed by contraction of capsular, or follicular intrinsic muscles (FMs) (Hill et al., 2008; Bosman et al., 2011). Whisker movement in caudal direction, or retraction, is provided by two EMs (*Mm. nasolabialis et maxillolabialis*) and elastic forces of the mystacial pad (MP) (Dörfl, 1982; Wineski, 1985). Dorsoventral movements are provided by another two EMs (*M. transversus nasi* et Pars orbicularis oris of the *M. buccinatorius*) (Dörfl, 1982; Bosman et al., 2011). Rolling of the whisker shaft around its own axis during whisking was described in behaving rats as torsional rotation by Knutsen and colleagues (Knutsen et al., 2008) who suggested that torsion may be caused by asymmetric motor innervation of the two extremities of FMs. Whisker torsion was suggested to be performed also by oblique intrinsic muscles (OMs) that were recently described in the two most dorsal whisker rows of the MP of the other whisking mammal, marsupial *Monodelphis domestica*, and in guinea pigs (Grant et al., 2013, 2017).

Visual perception, similar to vibrissa-based tactile perception, is obtained via sensory organ movements in three directions: horizontal, vertical and torsional (Tweed et al., 1990). For the vision, it was found that the coordination between the torsional and other movements of the eye is achieved, at least in part, via mechanical coupling that implements the Donders-Listing's law (Demer, 2002). Whether this is the case in the vibrissal system was not known. Moreover, it was not known whether vibrissal torsion is induced by asymmetries in the architecture or operation of the FMs and EMs, or by dedicated muscles as in the ocular system.

Whisking is extensively studied mainly in two rodent species, mice and rats. Nevertheless, up to date, there is no unanimous opinion, nor direct experimental data about muscular substrate that is responsible for the whisker torsion in both these species. In the current study, we revealed OMs that are present in the MP and may be responsible for whisker torsion in adult and newborn mice and rats. Each of these muscles possessed a cluster of neuromuscular junctions. Local electrical stimulation of OMs in adult rats provoked torsion of both adjacent whiskers.

MATERIALS AND METHODS

Animals

The animals were sixteen adult, four 2-week-old, and four 4-day-old albino Wistar rats, and ten adult and six newborn C57BL/6 mice. Animal maintenance, manipulations and procedures were conducted in accordance with the National Institutes of Health Guide for the Care and Use of Laboratory Animals and were approved by the Institutional Animal Care and Use Committee of The Weizmann Institute.

Staining for Cytochrome Oxidase (CCO) Activity

Mice and rats were anesthetized intraperitoneally with urethane [25% (w/v); 0.65 mL/100 g body weight], and perfused transcardially [4% (w/v) paraformaldehyde, and 5% (w/v) sucrose in 100 mM phosphate buffer, pH 7.4]. Then the animals were decapitated. The muscles of the MP were visualized by histoenzymatic reaction for CCO activity that was performed according to our modification (Haidarliu and Ahissar, 2001) of the procedure by Wong-Riley (1979). Briefly, after perfusion, MPs were excised and placed into 4% (w/v) paraformaldehyde solution with 30% (w/v) sucrose. After 48 hr of postfixation, MPs of adult mice and rats were cut tangentially, and entire heads of the 2-week-old rats, horizontally, into 60 μm thick slices for rats, and into 30 μm thick slices for mice, by using a sliding microtome (SM 2000R, Leica Instruments, Germany) coupled to a freezing unit (K400, Microm International, Germany). Free-floating slices were incubated in an oxygenated solution of 0.02% (w/v) cytochrome c (Sigma-Aldrich, St. Louis, MO, USA), catalase (200 μg/mL), and diaminobenzidine [0.05% (w/v)] in 100 mM phosphate buffer at room temperature under constant agitation. When a clear differentiation between highly-reactive and non-reactive tissue structures was observed, the incubation was arrested by adding 0.5 mL of 100 mM phosphate buffer into each of the incubation wells. Stained slices were washed, mounted on slides, cover-slipped with Entellan (Merck KGaA 64271 Darmstadt, Germany) and examined using a Nikon Eclipse 50i microscope. Bright-field images were imported into Adobe Photoshop software. Only minimal adjustments in the contrast and brightness of the images were made if needed.

Neuromuscular Junction Labeling

Motor end plates were revealed in the muscles of the mouse and rat MPs by staining for postsynaptic nicotinic acetylcholine receptors with rhodamin-conjugated α-bungarotoxin (BTX, Molecular probes, B-13422). Anesthetized rats were decapitated, and their MPs were excised and kept overnight in a solution of 4% paraformaldehyde with 30% sucrose at 4° C. Then the pads were washed in 0.1 M phosphate buffer and left overnight in a solution of 30% sucrose in PBS at 4°C. The samples were then cut tangentially into slices 60 μm thick, and incubated with BTX solution (1:200) for 1 hr at room temperature. In anesthetized adult mice and pups of both species, MPs were also excised, incubated in BTX (1:200) for 30 min at room temperature, and fixed for another 30 min in 4% paraformaldehyde. The samples were then washed with 0.1 M phosphate buffer, left overnight in a solution of 30% sucrose in 0.1 M phosphate buffer at 4° C, and cut tangentially into slices 40 μm thick. Then the slices of both mice and rats were placed on standard microscope glass slides and cover slipped with Vectashield (Vector Laboratories, Inc., Burlingame, CA). The slices were examined using a Nikon Eclipse 50i epifluorescence microscope, and the images were imported into Adobe

Photoshop software. For better visualization of the muscles that contain end plates, the slides were placed into saline and cover glasses removed. Then the slices were placed into wells and stained for CCO activity as described above.

Functional Assessment of OMs

In order to evaluate feasibility of OMs to generate whisker roll along the shaft (torsion), we applied electrical stimulation using bipolar microelectrodes. Six experiments were performed on male albino Wistar rats (b.w. 280–480 g) under urethane (1.5 g/kg, i.p.) anesthesia. Anesthetized rats were secured in anatomically adapted, earbar-free head holder that was mounted onto a stereotaxic instrument (SR-6; Narishige, Tokyo, Japan). The body temperature was monitored rectally and maintained at 37°C by servo-controlled heating blanket. To monitor and capture the whisker torsion, two 3–4 mm long pieces of a polyimide tubing (Translucent Anber Miniature Polyimide Tubing, 31 AVG, 0.0089″ ID, 0.0104″ OD, 0.00075″ Wall; Small Parts, Inc., Miami, FL, USA) were attached to each other to form a T-shaped connection. One of the tubings was threaded by a whisker and secured thereto by a tiny bead of superglue, whereas the other one served as a pointer for detecting whisker torsion. Intrinsic muscles were stimulated through bipolar tungsten parallel microelectrodes (30–50 μm exposed tip diameters, 100–200 μm distance between the tips) that were inserted through a small incision in the epidermal layer of the skin between two neighboring follicles of the same row. The point of penetration was shifted by ~0.5 mm dorsal to the line formed by the whiskers in a row, and the electrode was tilted dorsally so that it would reach the depth of ~1.5 mm between adjacent follicles that corresponds to the location of OM bellies in rats. Our goal in these experiments was to activate selectively OMs. The microstimulation parameters were selected in a way to get maximal torsion effect and to restrict the contraction of functionally different surrounding muscles. We applied 1–4 sec trains of muscle microstimulation with a frequency 2–5 Hz and duty cycle 100–140 ms. Biphasic rectangular electrical pulses (10–140 μs duration) were applied through an isolated pulse stimulator (Model 2100; A-M systems, Sequim, Washington, United States) at frequencies 50–83 Hz that produce a smooth contraction of the muscles (Szwed et al., 2003). The current between 50 and 150 μA generated a well-defined torsion that was accompanied by simultaneous moderate protraction of the adjacent whiskers. Whisker movements were recorded at 1,000 frames/s with a fast digital video camera (AOS-X-PR1, AOS Technologies America, Inc. San Jose). Whisker torsion and protraction were analyzed offline using image processing software (Knutsen et al., 2005). Periods corresponding to the torsion and protraction cycle-duration (starting from the first frame through the video clip) were extracted automatically, filtered (low pass cut-off −20 Hz), averaged using custom-written MATLAB software (Knutsen et al., 2005) and subjected to further analysis. For every whisker captured in the video, a three-point piecewise polynomial (spline) was fitted to the horizontal projections of whisker profiles. The whisker angle was computed from the spline at the base of the tracked whisker from the coefficients of the most proximal polynomial of the whisker-spline representation (Bagdasarian et al., 2013). Whisk amplitude was defined as protraction amplitude, and whisk duration was defined as combined duration of protraction and retraction. Set-point was the angle at the protraction onset. Mean torsion and mean protraction values of averaged angles trajectories were calculated for each whisker in 20–100 ms time interval after the stimulus onset.

At the end of each experimental session, electrolytic lesions were produced by passing current (100 μA, 16 s, unipolar) through the tips of the stimulating electrodes. The lesions of the stimulated sites were clearly visible in stained for CCO activity tangential slices of the MP that allowed spatial reconstruction of the electrode tip location in a stimulated muscle.

Estimation of Whisker Torsion in Pups

Mouse pups on the day of delivery (P0) and 1-day-old (P1) were placed on a small platform and heated by an infrared lamp. When the mice were falling asleep, their whiskers were sporadically performing spontaneous movements which were recorded at 200 frames/s for 1 hr by a high-speed camera (Optronis CL600x2) under IR illumination (880 nm). The control for head movements occurred during the recording, as well as during the process of estimation of the torsional movements. During recording, the pups were asleep, and the camera was focused on the snout region. If the head (snout) moved, recording was stopped until the movement ceased, then recording was continued. During estimation of the torsional movements, the images from each pre- and post-movements were superimposed, and the images with whatever change in the snout shape or position were omitted from the analysis.

Whisker movements were asynchronous and involved single or groups of whiskers that resembled twitches described in 3–6-day-old rats by Tiriac and colleagues (Tiriac et al., 2012). Some of the whiskers were changing the top-projected intrinsic curvature. Such changes of the top projection of the whisker curvature were considered by Knutsen and colleagues (Knutsen et al., 2008) a reliable indicator of their torsional rotation because intrinsic shape of the whisker shaft does not change during whisker movement, and no translation of the whisker pad was observed. To determine the degree of whisker torsion, we calculated the top-projected curvature along the whisker shaft both in resting whisker and when it performed a torsional twitch, by using the equation ($ktop = 1/r$) proposed by Knutsen and colleagues (Knutsen et al., 2008), and the calibration curve for the torsion in the range between 50 and 90°, in which the relationship between the angle of torsion and top-projected curvature was shown to be linear (Knutsen et al., 2008).

RESULTS

Localization of OMs in Mice

In tangentially cut slices of the mouse MP, whisker follicles were neatly organized in five rows which were caudally framed with the follicles of four straddlers (Fig. 1a,c). Within the rows, adjacent whisker follicles were interconnected by FMs whose appearance corresponded to their classical description (Dörfl, 1982). Each of the

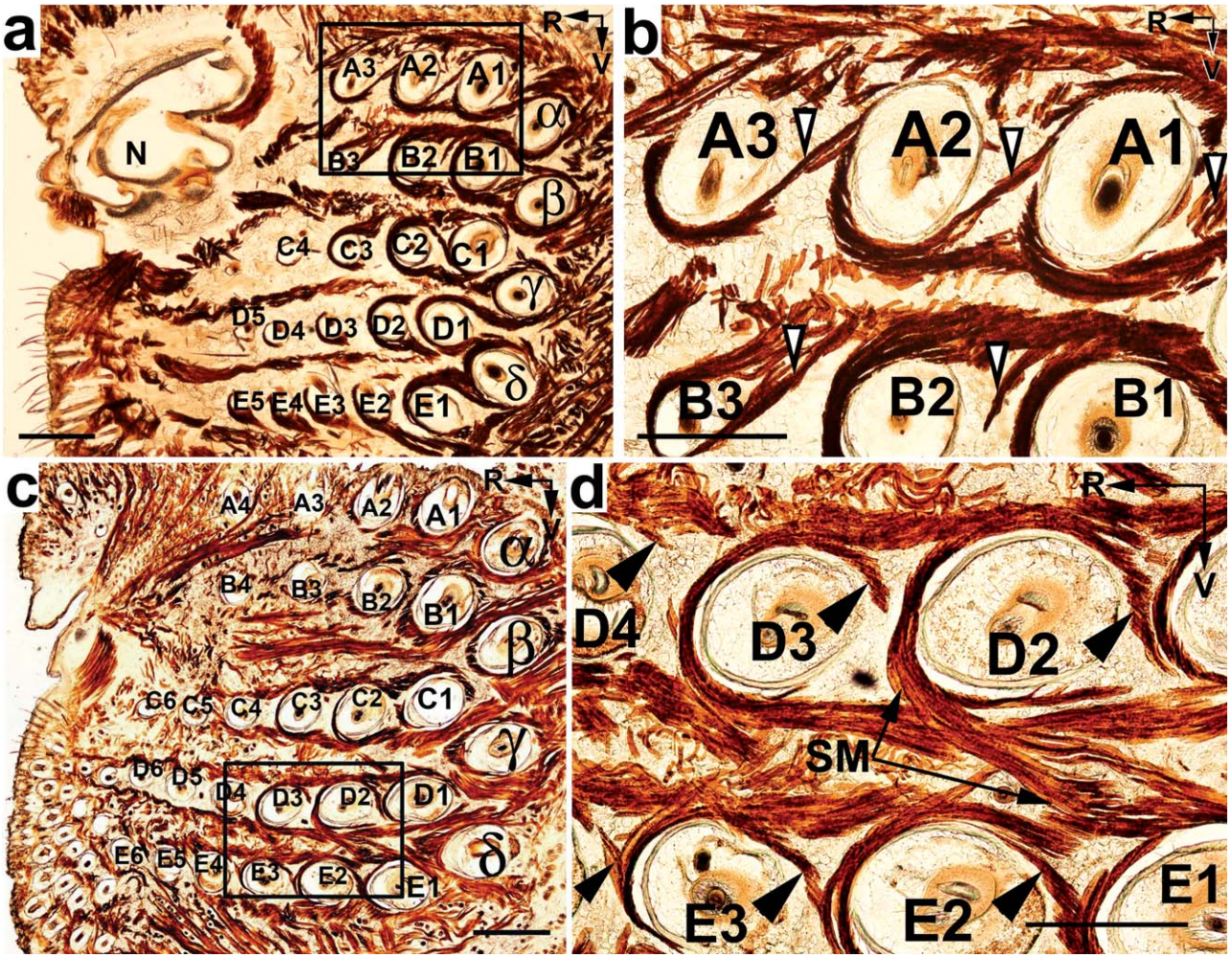

Fig. 1. Light microscopy of the tangential slices (a and c) of the MP in adult mice. (b, d) Enlarged boxed areas in (a) and (c) that contain OMs of the nasal and maxillary compartments of the MP, respectively. Staining for CCO activity. A1 – E6, whisker follicles; α – δ, straddler follicles; N, nasal cavity; R, rostral; V, ventral. Arrow heads point at OMs. Scale bars = 1 mm.

FMs originated from the rostral surface of the proximal segment of mystacial whisker follicles. The two extremities of FMs were directed caudolaterally along the rows of the whisker follicles, and were inserted into the distal end of a more caudally located follicle and adjacent corium. Within the spaces between neighboring follicles in a row, we revealed OMs that were crossing these spaces diagonally. In the rows A and B, OMs originated from the ventral surface of a rostrally located whisker follicle, continued their way in the dorsocaudal direction between the two follicles in a row, and inserted into the dorsal surface of the distal end of the neighboring, caudally located whisker follicle (Fig. 1b). The belly of OMs was entirely between the whisker follicles within a row. According to the position of the origins and insertion sites of the OMs, their contraction will rotate the whisker shafts of the rows A and B about their own axes in the right MP, when looking from the tip of the whisker back toward the base, clockwise, and in the left MP, counterclockwise.

In the rows C–E, OMs originated from the dorsal surface of the rostral whisker follicle, passed between the two neighboring follicles in the ventrocaudal direction, and inserted into the ventral surface of the distal end of the neighboring, caudally located whisker follicle close to the corium (Fig. 1d). We suggest that contraction of the OMs in the maxillary compartment of the MP (rows C, D, E) will rotate the follicles in opposite direction compared to the rotation of the follicles in the nasal compartment of the MP (rows A and B). We revealed also a "straddling" intrinsic muscle (SM) that connects follicles of the two adjacent whisker rows (Fig. 1d), similar to those described by Yohro (1977).

Localization of OMs in Rats

Rats possessed a similar to mice arrangement of the whisker follicles, FMs, and OMs (Fig. 2a,c). In the nasal compartment of the MP in rats, similar to mice, OMs originated from the ventral side of the rostral follicle, and inserted into the dorsal side of the adjacent caudal follicle (Fig. 2b), whereas in the maxillary compartment, OMs originated from the dorsal side of the rostral follicle, and inserted into the ventral side of the adjacent caudal follicle in a row (Fig. 2d). We suggest that

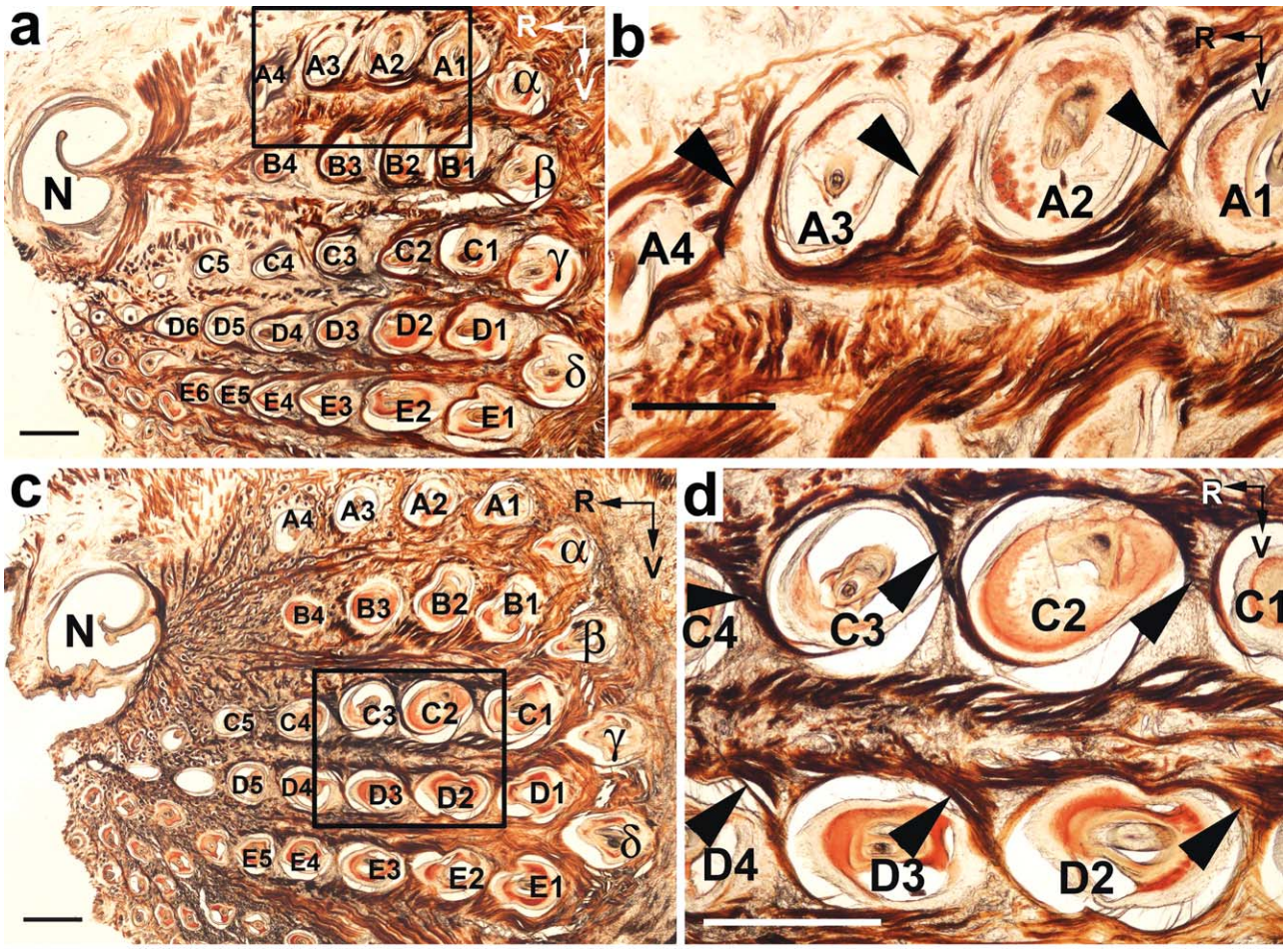

Fig. 2. Light microscopy of the tangential slices (a and c) of the MP in adult rats. (b, d) Enlarged boxed areas in (a) and (c) that contain OMs of the nasal and maxillary compartments of the MP, respectively. Staining for CCO activity. A1 – E6, whisker follicles; α – δ, straddler follicles; N, nasal cavity; R, rostral; V, ventral. Arrow heads point at OMs. Scale bars = 1 mm.

contraction of the OMs in rats, similar to mice, will provoke torsion of the whiskers in these compartments in opposite directions.

Tangential slices of the rat MP contained entire set of whisker follicles, but usually only one of the two compartments contained OMs. This can be explained by the convex shape of the MP that interferes with obtaining entire set of OMs in a single slice, as well as by the separation of the MP into two parts by the nasolacrimal groove that is seen clearly in the embryonal (E12) rat (Erzurumlu and Jhaveri, 1992) and fuzzily, but still observable, in adults (Fig. 3a). The layout of the OMs in the entire rat MP and their different orientation in the two compartments of the MP is shown schematically in Figure 3b.

Horizontal slices of the snout of two-week-old rats contained only one or two rows of whisker follicles. In such slices, OMs were revealed also within the spaces between adjacent follicles. The long axes of the follicles in row A were directed dorsally, so that they were cut transversally or under a small angle (Fig. 4a). In the row A, both FMs and OMs were revealed in the same slices (Fig. 4b). In adult rats, OMs also can be revealed in the horizontal slices of the MP. In Figure 4c, the bellies of the OMs are crossing the spaces between adjacent follicles in a row at a depth of up to ~1 mm from the surface of the skin, then muscle fibers are directed caudally and more superficially where they insert into the distal ends of the caudally located adjacent follicles.

Motor Innervation of Intrinsic Muscles

Motor end plates were revealed in all intrinsic muscles of the MP (Fig. 5). In the OMs, end plates were forming small clusters that were observed in the spaces between neighboring follicles in a row. Distribution of the motor end plates confirmed the differences in the position of OMs in the nasal (Fig. 5a,c) and maxillary (Fig. 5b,d) compartments of the MP in both mice and rats. In the FMs, end plates were forming large clusters that were located in both extremities of each FM. The extremities of FMs in fact were running within the spaces between the rows of whisker follicles. Motor end plates were also observed in SMs.

Effects of Electrical Microstimulation of OMs

Electrical stimulation of OMs was performed by bipolar microelectrodes that were inserted into the spaces

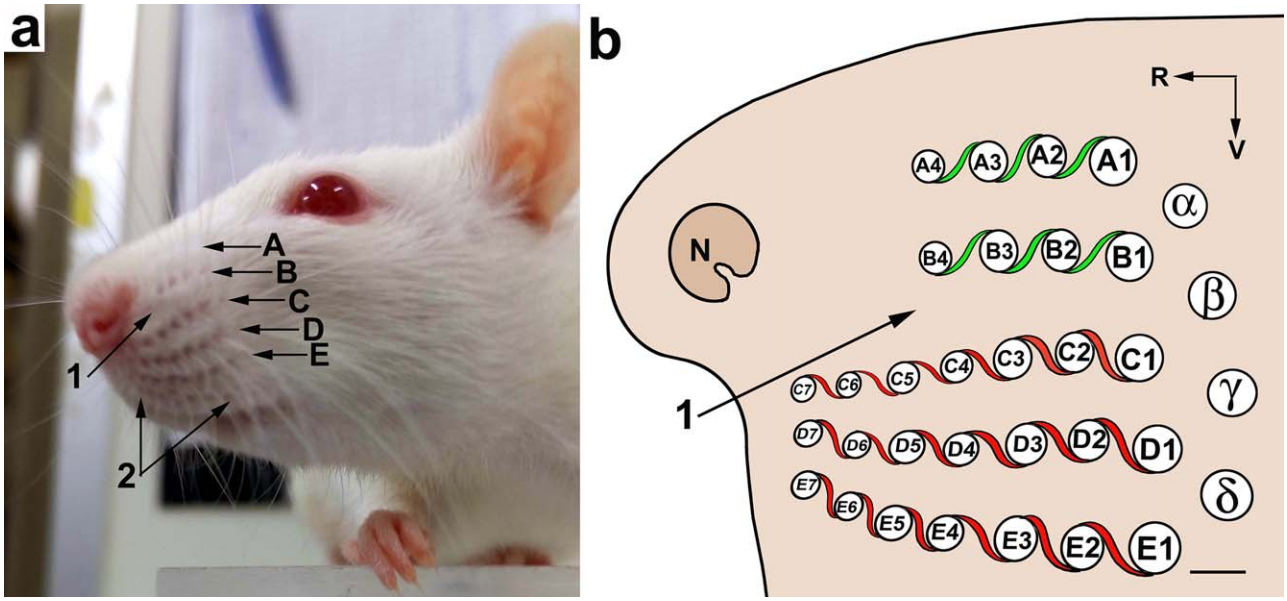

Fig. 3. Compartmentalization of the MP in rats. (a) A photograph of the head of an adult rat. (b) Schematic representation of the OMs in the nasal (green filling) and maxillary (red filling) compartments of the rat MP. (α – δ) Straddler follicles; A1 – B4, follicles of the nasal compartment of the MP; C1 – E7, follicles of the maxillary compartment of the MP. N, nostril. R, rostral; V, ventral. (1) nasolacrimal groove; (2) furry buccal pad. Scale bar = 1 mm.

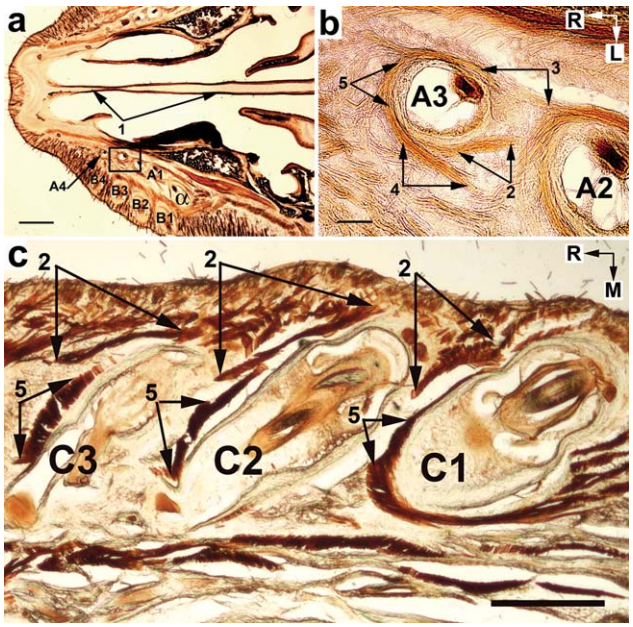

Fig. 4. Horizontal slices of the snout of a 4-week-old rat (a and b) and of the MP of an adult rat (c). (1) Septum; (2) OMs; (3 and 4) dorsal and ventral extremities, respectively, of the FM of the follicle A3; (5) arcs of the FMs; α, straddler; A1 – C3, whisker follicles; L, lateral; M, medial; R, rostral. Scale bars = 1 mm (a and c), and 0.1 mm (b).

between neighboring whiskers of the same row to the depth of 0.25–2.0 mm. When the electrode tip was located exactly within an OM, electrical stimulation resulted in torsion of both adjacent whiskers in the same direction and small whisker protraction. The snapshots shown in Figure 6a demonstrate whisker position before and after stimulation of the OM that connects whisker follicles C2 and C3. When these two snapshots were superimposed, whisker torsion could be clearly seen according to the differences in the position of polyimide tubings. Average angles of the torsion and protraction of the same whiskers are shown in Figure 6b. Schematic drawing of the stimulation site within the OM (Inset in Fig. 6b) is based on histologically verified location of stimulating electrode tips (Fig. 6c,d).

The mean angle (see "Methods") of whisker torsion that was measured in 35 whiskers, ranged from −2.79 to 15.3°. Examples of the average torsion angles and the histogram of torsion mean angle frequency distribution are shown in Figure 7a,b. As with intact behaving rats (Knutsen et al., 2008), also with direct electrical stimulation of OMs in the MP of anesthetized rats, whisker torsion was usually accompanied with moderate whisker protraction (Figs. 6b and 7a). However, it should be emphasized that in contrast to behaving rats, the ratio between torsion and protraction evoked by direct electrical microstimulation of the muscles in anesthetized rats depends on various factors, such as geometry of the tissues surrounding the electrode, magnitude of the stimulating current, distance between the electrode tips, location of stimulation, as well as impeding mechanical action of the other follicles in a row. Due to mentioned factors it was difficult to determine a real relationship between torsion and protraction during application of the direct stimulation to the muscle.

Whisker Torsion and MP Musculature in Pups

Sleeping newborn mice (P0) were video-recorded from top while performing sporadic asynchronous whisker movements of which a part was estimated as a torsional rotation. During whisker torsion, the projection of its

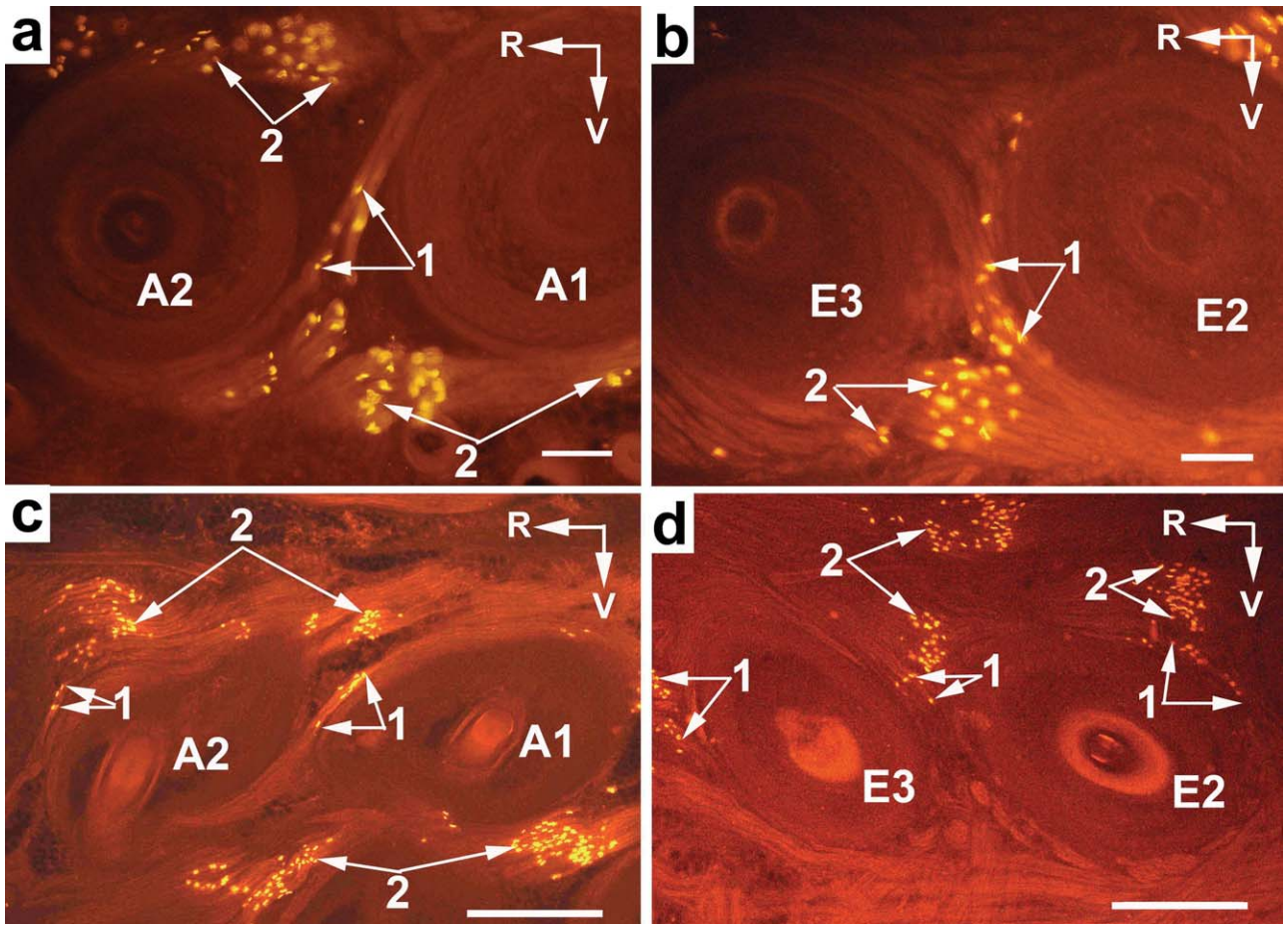

Fig. 5. Distribution of motor end plates in intrinsic muscles of a mouse (a and b) and of a rat (c and d) MPs. Staining with rhodamin-conjugated bungarotoxin. A1, A2, E2, E3, whisker follicles; (1) end plates in OMs; (2) end plates in FMs. R, rostral; V, ventral. Scale bars = 0.1 mm (a and b) and 0.5 mm (c and d).

intrinsic curvature on the horizontal plane, that is captured by the video camera, changes. Such changes of the projected whisker curvature and of its angle of torsion were shown to be linear in the range between 50 and 90° of torsion (Knutsen et al., 2008). We registered eight torsional twitches with the mean duration of a single torsion 0.6 sec. One example of the whisker torsional twitch is shown in Figure 8a–c. The changes in the projected curvatures of the whiskers that were observed during performance of the rotational twitches were measured, and the angles of torsion were determined by using the relationship reported by Knutsen and colleagues (Knutsen et al., 2008) and shown in Figure 8d. In the example of the whisker torsion shown in this figure, projected curvatures of the resting whiskers diminished during rotational twitches by 3 mm^{-1} for the whisker C3, and by 4 mm^{-1} for the whisker C4, which correspond to their torsional rotation by 6.7° and 8.7°, respectively.

Torsional movements occurred in pups spontaneously while they were sleeping. These torsional movements were coupled with slight protraction of the two adjacent whiskers, and such movements were performed independently on the movements of other whiskers.

In newborn (P0–P4) mice and rats, the musculature of the MPs was visualized in tangential slices by staining for CCO activity. The composition and distribution of the muscles in pups was similar to that in adult animals: the types of intrinsic muscles (FMs and OMs), as well as superficial and deep whisker protracting and retracting muscles were revealed in pups of both mice (Fig. 9a) and rats (Fig. 9d). The OMs were represented by muscle bundles that connected diagonally adjacent whisker follicles in a row both in mice (Fig. 9b) and rats (Fig. 9e). In both species, OMs and FMs were provided with motor innervation (Fig. 9c,f).

DISCUSSION

Organization of Intrinsic Muscles within the Rodent MP

In the rodent MP, three types of intrinsic muscles were revealed: FMs, SMs, and OMs. FMs were mentioned more than 100 years ago as flat bands of striated muscle fibers that surround whisker follicles on three sides (Vincent, 1912). Later Dörfl (1982) named these muscles “follicular” and described them as slings composed of an arc that surrounds the lower third of the rostral member of every pair

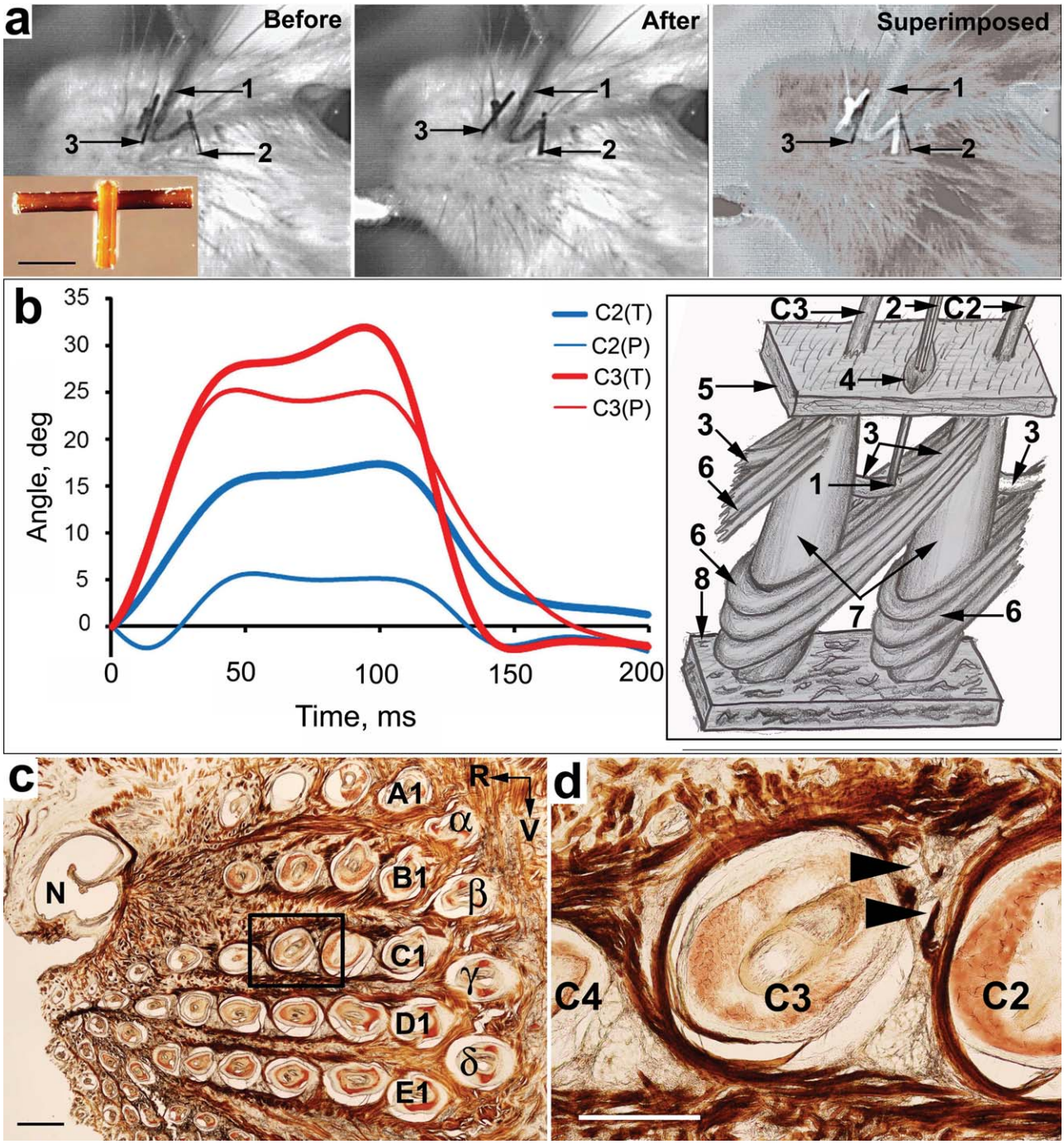

Fig. 6. Effect of electrical stimulation of the OM that connects whisker follicles C2 and C3 in the rat MP. (a) Separate and superimposed snapshots showing the position of polyimide tubings attached to the whiskers C2 (2) and C3 (3) before and after microstimulation by a bipolar electrode (1). (b) Average angles of torsion (T) and protraction (P) of the whiskers C2 and C3 during stimulation of their common OM. (c) Tangential slice of the MP stained for CCO activity. (α – δ) Straddler follicles; A1 – E1, whisker follicles. Scale bar = 1 mm. (d) Enlarged boxed area in (c), with two lesions (arrow heads) in the OM between whiskers C2 and C3. Scale bar = 0.5 mm. **Inset** in (a): Polyimide tubings attached perpendicularly to each other (see "Methods" for details). Scale bar = 1mm. Inset in (b): Schematic drawing that shows the site of stimulation (1) by a bipolar electrode (2) within the OM (3); (4) incision in the epidermal layer of the skin (5); (6) FMs; (7) whisker follicles; (8) deep fibrous mat.

of follicles in a row, and two extremities that insert into the dorsal and ventral faces of the distal end of the caudal follicle and adjacent corium. These muscles are also known as "capsular" (Jin et al., 2004, Bosman et al., 2011) or "sling" muscles (Hobbs et al., 2016), and are defined as vibrissal protractors.

Another type of intrinsic muscles, SMs, was observed in the maxillary compartment of the MP of the big-

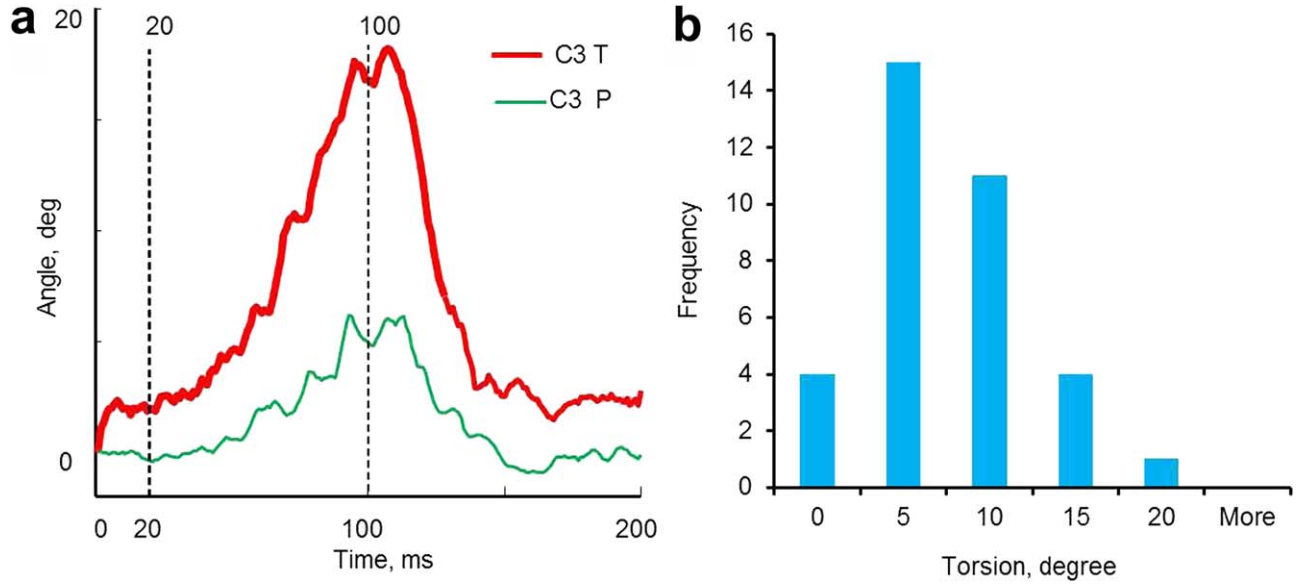

Fig. 7. Effect of electrical microstimulation of the OMs on whisker torsion. (a) Average torsion (T) and protraction (P) angle trajectories of the two C3 whiskers evoked by OM microstimulation at the depth ~1mm from the surface of the MP in different experiments. Mean torsion and mean protraction values of averaged angle trajectories were calculated for each whisker in 20–100 ms time interval [dashed lines in (a)] after the stimulus onset. (b) Histogram of torsion mean angle frequency distribution of 35 whiskers.

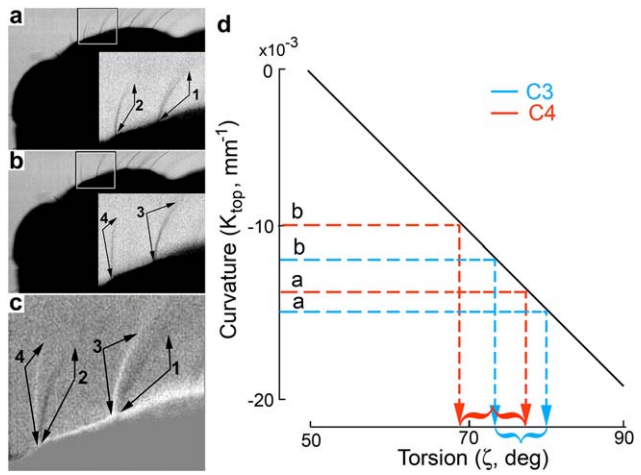

Fig. 8. High-speed recording of whisker movement in 1-day-old mouse. (a) Resting whiskers; (b) same whiskers performing a rotational twitch. Insets in (a) and (b) represent enlarged boxed areas in the same panels. (c) Superposition of the Inset in panel (a) by the semi-transparent inverted Inset in panel (b). (d) Estimation of the angles of torsion of the whiskers C3 and C4 by measuring the top-down projected curvatures (k_{top}) of the resting (a) and twitched (b) whiskers C3 (blue) and C4 (red). (1 and 2) Whiskers in resting position; (3 and 4) the same whiskers performing a rotational twitch.

clawed shrew by Yohro (1977). These muscles are forming bridges in a hexagonal manner between the follicles of the neighboring ventral whisker rows. Similar SMs were recently described by Grant and colleagues between the ventral rows of the MP in marsupial *Monodelphis domestica* and in guinea pigs (Grant et al., 2013, 2017). We also observed SMs in the maxillary compartment of the mouse MP. As the functional aspects of the SMs were not yet described, only FMs are considered to represent intrinsic musculature of the MP that participates in whisker protraction.

In addition to FMs and SMs, auxiliary intrinsic muscles were recently observed between adjacent follicles within the two dorsal whisker rows (nasal compartment of the MP) of the marsupial *Monodelphis domestica* and guinea pigs (Grant et al., 2013, 2017). These muscles were diagonally crossing the spaces between adjacent follicles, and were named OMs. In the current study we revealed similar OMs, but they were present in both nasal and maxillary compartments of the MP in mice and rats. These muscles were composed of few muscle bundles that were crossing diagonally the spaces between neighboring whisker follicles in each whisker row. They originated from the ventral (rows A and B) or dorsal (rows C, D and E) sides of the rostrally located follicles, and inserted into the opposite sides of adjacent, caudally located follicles.

Intrinsic muscles of the mammalian MP have separate origins and insertion sites on the vibrissa capsules, and possess separate sets of neuromuscular junctions. Taken together, intrinsic musculature of the MP can be considered a muscular ensemble that is involved not only in the rostro-caudal whisker motion, but also in implementation of sophisticated whisker behavior by supplementary rolling of the whiskers about their own axes, divergence of adjacent whiskers and dorso-ventral elevation which were already described in experiments with rodents (Bermejo et al., 2002; Sachdev et al., 2002;. Knutsen et al., 2008) and confirmed by modeling whisker kinematics (Hobbs et al., 2012; Huet and Hartmann, 2014).

Effects of Direct OM Microstimulation on Whisker Behavior

The fact that direct electrical stimulation of OMs in anesthetized rats rolls adjacent whiskers about their

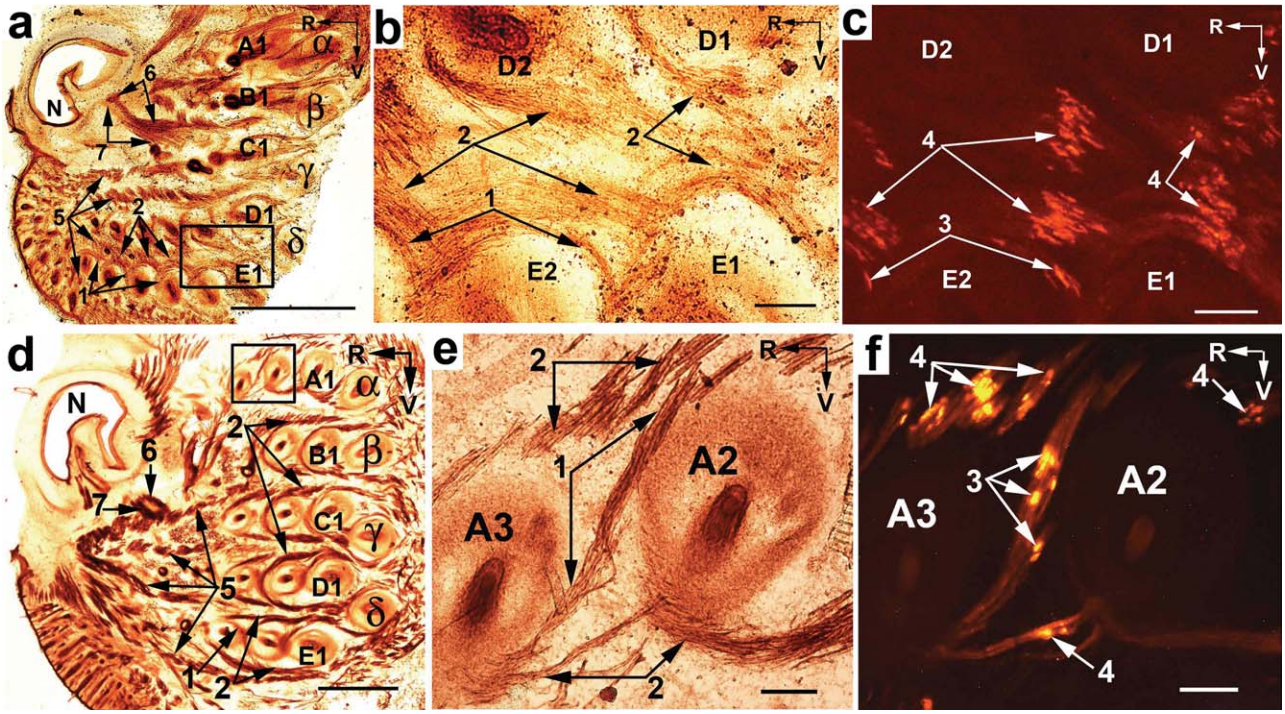

Fig. 9. Musculature of the MP in a new-born (P0) mouse (a–c) and in a 4-day-old rat (d–f). Staining for CCO activity (a, b, d, e) and for nicotinic acetylcholine receptors (c, f). (a, d) Tangential slices of the MP; (b, e) enlarged boxed areas in (a) and (d), respectively; (c, f) end plates in the OM and FMs shown in (b) and (e), respectively. (1) OMs; (2) FMs; (3) and (4) end plates in the OMs and FMs, respectively; (5, 6, and 7) Pars media inferior and Partes maxillares superficialis et profunda, respectively, of the *M. nasolabialis profundus*. Scale bars = 1 mm (a, d), and 0.1 mm (b, c, e, f).

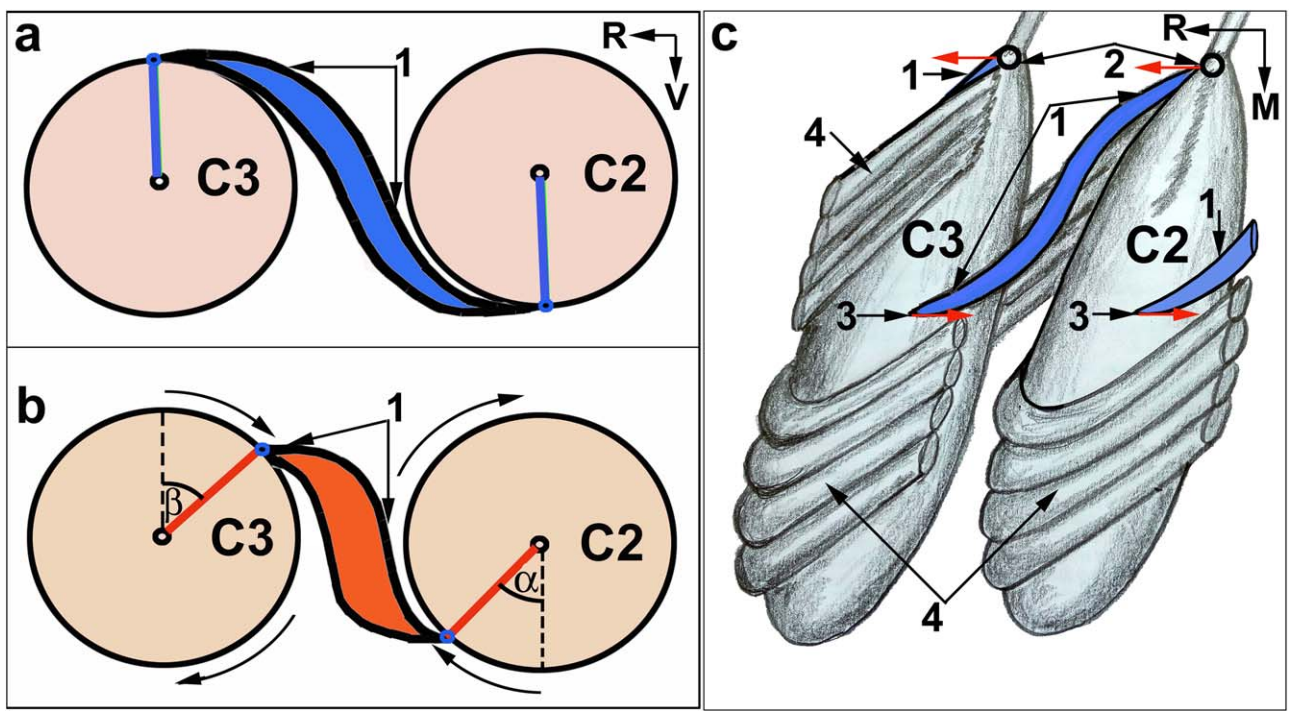

Fig. 10. Suggested mechanism of whisker torsion (a and b) and of protraction (c) during microstimulation of an OM. (1) OMs: blue filling = relaxed, red filling = contracted; (2) whisker pivot points; (3) OM origin; (4) FMs. (α and β) Angles of torsion of the whisker follicles C2 and C3, respectively. Curved arrows indicate the direction of torsion, red arrows show direction of pulling the follicles that causes whisker protraction. M, medial; R, rostral; V, ventral.

long axes, and that these muscles are supplied with motor innervation suggests that OMs represent the muscular substrate of the whisker torsion. However, stimulated OMs not only rolled adjacent whiskers about their own axes, but also protracted them. To understand the mechanism of the simultaneous whisker torsion and protraction, it is necessary to address spatial relationships of the OMs with the follicles and geometry of the sites of OMs attachment to the follicles. Whisker torsion appears as a result of the tangential pulling when the force is applied to the opposite sides of the two adjacent follicles (Fig. 10a,b), whereas protraction mechanism of the OMs is similar to that of the FMs (Dörfl, 1982). Attachment of an OM to the rostral follicle (origin) is located proximal to the whisker pivot point, so it pulls the proximal end of the follicle caudally causing whisker protraction, while the insertion site is located on the distal end of the caudal follicle, so it pulls it rostrally, also causing protraction of the caudal whisker (Fig. 10c).

Knutsen and colleagues (Knutsen et al., 2008) found that in adult behaving rats torsion is consistently coupled with a significant protraction across whisking epochs. Based on the current results we hypothesize that the strong coupling during behavior is based not solely on the function of the musculature that is dedicated to torsion, as this alone provides only moderate protraction, but rather that it involves significant degree of coordinated neuronal control of FMs and OMs.

CONCLUSIONS

1. Mystacial pads of newborn and adult mice and rats contain OMs that are innervated by motor neuron's axonal terminals and cause whisker torsion.
2. Torsional twitches in newborn pups occur before emergence of whisking.
3. Whisker torsion is mechanically coupled to some degree to whisker protraction, not sufficiently to account for the observed behavioral coordination.
4. The morphology of the OMs determines the direction of torsion. Inverse insertion patterns induce inverse torsion of the whiskers in the rows A-B versus rows C-E.

COMPETING INTERESTS

No competing interests declared.

ACKNOWLEDGMENTS

The authors would like to thank Dr. Raya Eilam-Altstadter for her help and guidance of histochemical techniques.

LITERATURE CITED

Bagdasarian K, Szwed M, Knutsen PM, Deutsch D, Derdikman D, Pietr M, Simony E, Ahissar E. 2013. Pre-neuronal morphological processing of object location by individual whiskers. Nat Neurosci 16:622–631.

Bermejo R, Vyas A, Zeigler HP. 2002. Topography of rodent whisking–I. Two-dimensional monitoring of whisker movements. Somatosens Mot Res 19:341–346.

Bosman LWJ, Houweiling AR, Owens CB, Tanke N, Shevchouk OT, Rahmati N, Teunissen WHT, Ju C, Gong W, Koekkoek SKE, et al. 2011. Anatomical pathways involved in generating and sensing rhythmic whisker movements. Front Integr Neurosci 5:53.

Demer JL. 2002. The orbital pulley system: a revolution in concepts of orbital anatomy. Ann N Y Acad Sci 956:17–32.

Dörfl J. 1982. The musculature of the mystacial vibrissae of the white mouse. J Anat 135:147–154.

Erzurumlu RS, Jhaveri S. 1992. Trigeminal ganglion cell processes are spatially ordered prior to the differentiation of the vibrissa pad. J Neurosci 12:3946–3955.

Grant RA, Haidarliu S, Kennerley NJ, Prescott TJ. 2013. The evolution of active vibrissal sensing in mammals: Evidence from vibrissal musculature and function in the marsupial opossum Monodelphis domestica. J Exp Biol 216:3483–3494.

Grant RA, Delaunay MG, Haidarliu S. 2017. Mystacial whisker layout and musculature in the guinea pig (*Cavia porcell*us): a social, diurnal mammal. Anat Rec (In Press).

Haidarliu S, Ahissar E. 2001. Size gradients of barreloids in the rat thalamus. J Comp Neurol 429:372–387.

Hill DN, Bermejo R, Zeigler HP, Kleinfeld D. 2008. Biomechanics of the vibrissa motor plant in rat: rhythmic whisking consists of triphasic neuromuscular activity. J Neurosci 28:3438–3455.

Hobbs JA, Towal RB, Hartmann MJZ. 2016. Evidence for functional groupings of vibrissae across the rodent mystacial pad. PLoS Comput Biol 12:e1004109. doi: 10.1371/journal.pcbi.1004109.

Huet LA, Hartmann MJZ. 2014. The search space of the rat during whisking behavior. J Exp Biol 217:3365–3376.

Jin T-E, Witzemann V, Brecht M. 2004. Fiber types of the intrinsic whisker muscle and whisking behavior. J Neurosci 24:3386–3393.

Knutsen PM, Derdikman D, Ahissar E. 2005. Tracking whisker and head movements in unrestrained behaving rodents. J Neurophysiol 93:2294–2301.

Knutsen PM, Biess A, Ahissar E. 2008. Vibrissal kinematics in 3D: tight coupling of azimuth, elevation, and torsion across different whisking modes. Neuron 59:35–42.

Sachdev RN, Sato T, Ebner FF. 2002. Divergent movement of adjacent whiskers. J Neurophysiol 87:1440–1448.

Szwed M, Bagdasarian K, Ahissar E. 2003. Encoding of vibrissal active touch. Neuron 40:621–630.

Tiriac A, Uitermarkt BD, Fanning AS, Sokoloff G, Blumberg MS. 2012. Rapid whisker movement in sleeping newborn rats. Curr Biol 22:2075–2080.

Tweed D, Cadera W, Vilis T. 1990. Computing three-dimensional eye position quaternions and eye velocity from search coil signals. Vision Res 30:97–110.

Vincent SB. 1912. The function of vibrissae in the behavior of the white rat. Behav Monog 1:1–81.

Welker WI. 1964. Analysis of sniffing of the albino rat. Behavior 22: 223–244.

Wineski LE. 1985. Facial morphology and vibrissal movement in the golden hamster. J Morphol 183:199–217.

Wong-Riley M. 1979. Changes in the visual system of monocularly sutured or enucleated cats demostrable with cytochrome oxidase histochemistry. Brain Res 171:11–28.

Yohro T. 1977. Arrangement and structure of sinus hair muscles in the big-clawed shrew, Sorex unguiculatus. J Morphol 153:317–331.